Progress In Electromagnetics Research C, Vol. 87, 119–133, 2018

Through the Wall Imaging of Human Vital Signs Based on UWB MIMO Bioradar

Fulai Liang†, Miao Liu†, Fugui Qi, Hao Lv, Huijun Xue, Guohua Lu*, and Jianqi Wang*

Abstract—Through-the-wall imaging (TWI) of human vital signs by bioradar is a hot research topic in recent years. Unknown wall parameters (mainly thickness and dielectric constant) are huge challenges for TWI. Ambiguities in wall parameters will degrade the image focusing quality, lower signal-to-noise-clutter ratio (SNCR) of vital signs, cause vital signs to be imaged away from their true positions and blur the close vital signs from multiple humans caused by the imaging resolution declination. A through-the-wall propagation model of vital signs for multiple-input and multiple-output (MIMO) bioradar is first built to analyze the influence of wall on imaging. In order to obtain focused image of vital signs quickly, an imaging model and a novel autofocusing imaging method of vital signs are proposed in this paper. Since vital signs of human are weak and sensitive to interferences, the SNCR-enhanced imagery of vital signs after change detection (CD) is applied to evaluate the focusing quality of image. Reflections of wall in the stationary targets imaging result are line structure approximately, so Hough transform is used to extract the positions of the front edge and rear edge of wall automatically. Propagation time in the wall of electromagnetic waves is estimated and used to build the constraint relationship of wall parameters. The number of unknown parameters is reduced to only one and the efficiency of autofocusing imaging improves. Several cases, including the case of single human, multiple human objects close to each other and the case of non-human objects, are simulated. The magnetic resonance imaging (MRI) image of human chest is put into simulation scene. And then the simulation data of human vital signs are calculated by the finite-difference time-domain (FDTD) method. The results show that the proposed method can effectively estimate the wall parameters and improve the focusing performance of human vital signs. And also the kurtosis of image can be used as a feature to efficiently decide the human vital signs are existed or not. Thus the SNCR of vital signs and resolution of imaging are improved, which are beneficial for detection of vital signs. The position errors of human vital signs are also corrected.

1. INTRODUCTION

Bioradar technology has been widely applied to the areas such as noncontact medical measurement, through-the-wall surveillance and post-disaster rescue operation [1–4]. Bioradar-based detection and localization of multiple human targets through the wall is an emerging technology that has lots of civilian and military applications [5, 6].

With high penetrability and range resolution, ultra-wideband (UWB) waveform has the ability to determine the distance of vital signs with high accuracy and track the small movements of the diaphragm during breathing [3, 4]. However, most of these UWB systems use a single input and single output (SISO) channel, in which only range profile image of humans from single sight angle can be obtained. For the applications of non-line-of-sight (NLOS), the detection performance of SISO degrades [7]. A

Received 20 June 2018, Accepted 16 August 2018, Scheduled 27 September 2018

* Corresponding author: Jianqi Wang (fmmuwangjianqi@126.com); Guohua Lu (lugh1976@fmmu.edu.cn).
The authors are with the Department of Medical Electronics, School of Biomedical Engineering, Fourth Military Medical University, Xian 710032, China. † The first two authors Fulai Liang and Miao Liu contributed equally to this work.

natural idea to improve the through-the-wall detection and localization performance is to form high-resolution image of vital signs by through-the-wall imaging (TWI). TWI of human has been discussed in many papers [8–13]. [8, 9] detect and track moving human objects behind a wall. [10, 11] utilize the micro-motion of human body to reconstruct a human-body-enhanced composite image. Actually the micro-movement of body can also be seen as one type of human vital signs and usually used as an efficient feature to detect the existence of human being. When the human body is stationary, the vital signs mainly include the respiration and heartbeat. The micro-motion-enhanced TWI imagery of stationary human being is focused on these human vital signs [12, 13]. Through two-dimensional image, the shape and size of vital signs can be applied to detection, and two-dimensional localization can be obtained in the image [14].

There are two main different approaches of TWI of vital signs: synthetic aperture radar (SAR) imaging and multiple-input and multiple-output (MIMO) radar imaging. MIMO bioradar is a special type of multichannel radar which emerged in recent years. The MIMO array with M transmitting elements and N receiving elements can obtain a virtual aperture with $M \times N$ virtual transceivers, which greatly reduces the weight and cost of the radar system [15]. UWB MIMO radar combines the high range resolution property of the UWB signaling with the directional resolution property of the multiple antenna elements, so it has the potential of two-dimensional high-resolution imaging [16]. Compared with SAR, UWB MIMO bioradar can get multiple sight angles information of targets simultaneously and form high resolution image by one snapshot. Thus high resolution image sequence can be attained to describe the variation of the scenario. This advantage of the UWB MIMO bioradar makes it more proper for TWI of vital signs.

Mechanism of EM waves propagating in the air-to-wall-to-air medium is obviously different from that in the free space. When EM waves propagate in the wall, propagation velocity changes, and mutual inconsistence between channels emerges. The wall parameters, mainly wall thickness and dielectric constant, need to be precisely estimated for calibration. Ambiguities in the parameters will smear and blur the image and cause the imaged vital signs shift away from the true positions. When the wall is thin, or the dielectric constant of the wall has small value, only the shifting in range direction is observed and prone to be ignored. But when the wall is thick, or the dielectric constant of the wall is in large value, the dispersion of the image becomes severe which declines the resolution and signal-to-noise-clutter ratio (SNCR) of targets.

These effects will degrade the performance of TWI system. TWI system should be able to detect and classify vital signs in a populated scene with heavy static clutters, which may include interior back and side walls, waterpipes or various types of furniture items. And automatic detection of multiple human targets is a tougher problem due to the strong interference of clutters from other human bodies, such as the strong sidelobes and the shadowing effect. The dispersion effects of unknown wall parameters increase the difficulty of the accurate detection. It is of great importance for the system performance to be robust to ambiguities and inaccuracies in wall parameters.

Many efforts have been made to estimate the wall parameters. Transfer function of the wall is obtained by the time- or the frequency-domain measurement methods and used to estimate the wall parameters [17, 18]. However, these kinds of measurement methods require that two antennas are placed on different sides of the wall to obtain the transfer function. Therefore, these measurement methods are quite limited in practical situation. It is much more practical to estimate the wall parameters from the received echo without additional measurement.

Generally, the wall is considered as a uniform and regular medium. So the parameters of wall are simplified into the wall thickness and dielectric constant [19]. Several TWI techniques that provide correct target location without the knowledge of the wall parameters were proposed in [20]. These techniques require data to be acquired using at least two different array placement positions against the wall. At each position, imaging is performed for different values of wall thickness, and dielectric constant and target displacement trajectories are formed corresponding to a different position. The target position is then determined as the trajectories crossover point. However, the time duration of data collection increases since these techniques need changing the positions of antenna array. Thus, these techniques may be limited in practice.

Autofocusing method is a new method that relies on the idea that the focusing performance improves when the estimated wall parameters are close to the real ones [21]. No extra information

except echo data is needed to estimate the wall parameters. In SAR TWI of static targets, Jin et al. analyzed the propagation model of EM waves in the wall and proposed the processing schemes of two autofocusing algorithms [19]. Simulation results are given to prove the validity. However, this method cannot be directly used in vital signs imaging by UWB MIMO bioradar.

There are following differences between SAR TWI and vital signs TWI with UWB MIMO bioradar. Firstly, compared with TWI with SAR, UWB MIMO bioradar cannot be considered as monostatic radar any more. The propagation model needs to be reconsidered because the transmitting path and receiving path are different, and thus they should be computed respectively in the computation process of real electrical length. Secondly, the interested vital signs are weak targets. Thus, it is important to choose proper prominent targets to assess the focusing performance of image. The prominent targets should be with high SCNR and seen as point target. On one hand, the reflections of the wall are strong, but they are line structures in the image. On the other hand, the SNCR of interested vital signs is low and may not be suitable as prominent targets. It is necessary to enhance the SCNR of vital signs fully utilizing the motion information in autocuing method. Besides the above problems, computation acceleration of autofocusing iteration should be considered and well solved.

This paper is organized as follows. In Section 2, MIMO imaging model of vital signs in free space is discussed. Furthermore, through-the-wall MIMO imaging model of vital signs is analyzed in Section 3. Then an autofocusing frame of TWI suitable for vital signs is proposed in Section 4. Section 5 contains the simulation results and discussions. Conclusions are given in Section 6.

2. MIMO IMAGING MODEL OF VITAL SIGNS IN FREE SPACE

As shown in Fig. 1, when EM waves derived from the mth transmitting channel illuminates the human body, part of them will be reflected and received by the nth receiving channel. Due to respiration, the chest cavity expands and contracts periodically, so the round-trip distance $d(\tau)$ varies periodically around the nominal distance d_0 accordingly

$$d(\tau) = d_0 + d_b \sin(2\pi f_b \tau) \tag{1}$$

where τ represents the slow time which corresponds to the acquisition time of each range profile. The range profile represents the projection of the human target scattering centers on the radar line of sight. d_b is the amplitude of the chest wall displacement caused by respiration and f_b is the respiration frequency.

Assuming that there are M transmitting channels and N receiving channels, the transmitting elements sequentially emit a wideband signal $s_T(t)$, while the receiving elements sample the scattered

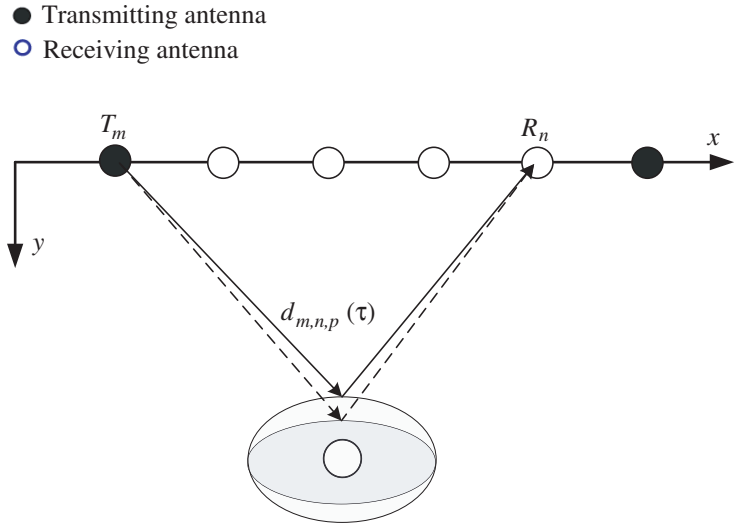

Figure 1. Model of vital signs in free space.

echoes simultaneously. t is the fast time which represents the time axis associated with range along each range profile. It can be thought orthogonal to the slow time dimension. The transmitting and receiving times of EM wave are so short that the frame rate of real bioradar is over 100 Hz. Thus, during each slow time, the vital signs are considered to be stationary and data from MN channels are seen to be collected simultaneously.

For each slow time, 2-D high-resolution image of interested human targets forms in the imaging plane x-y, where x and y denote the cross range and range, respectively. We can get the image sequence to illuminate the micro-motion of vital signs by arranging the images along slow time τ. The received signal collected by the mth transmitting antenna and the nth receiving antenna can be expressed as

$$s_{m,n}(t,\tau) = \sum_{p=1}^{P} s_T(t) \otimes h_p(t) \otimes \delta\left(t - \frac{d_{m,n,p}(\tau)}{c}\right) \tag{2}$$

where c is the speed of light in vacuum, $\delta(\cdot)$ the Dirac function, $\otimes$ the convolution operation, $h_p(t)$ the impulse response of the pth vital sign, $d_{m,n,p}(\tau)$ the round-trip distance between the pth human and the mth transmitting antenna and the nth receiving antenna.

In traditional image formations, it is often assumed that the EM waves propagate in a homogeneous medium. Therefore, the propagation path of the EM waves is a straight line between the antenna and the target.

Among the image formation methods, the back-projection (BP) imaging algorithm, which is well known for its high precision, simplicity and good adaptation to near-field imaging, is chosen as the basic imaging method in UWB MIMO TWI. At certain slow time τ_0, the BP algorithm is given as follows

$$I_{BP}(x,y,\tau_0) = \int \sum_{n=1}^{N} \sum_{m=1}^{M} s_{m,n}(t,\tau_0)\delta\left(t - \frac{l_{m,n}(x,y)}{c}\right)dt \tag{3}$$

where $l_{m,n}(x,y)$ represents the electrical length in free space from the pixel (x,y) and the mth transmitting antenna and the nth receiving antenna.

In free space, $l_{m,n}(x,y)$ is equal to the linear propagation distance

$$l_{m,n}(x,y) = \sqrt{(y-y_{T_m})^2 + (x-x_{T_m})^2} + \sqrt{(y-y_{R_n})^2 + (x-x_{R_n})^2} \tag{4}$$

where (x_{T_m}, y_{T_m}) is the position of the mth transmitted antenna, and (x_{R_n}, y_{R_n}) is the position of the nth receiving antenna.

If there exists a vital sign on pixel (x_0, y_0), $I_{BP}(x_0, y_0, \tau)$ illustrates its amplitude fluctuation caused by micro-motion can be used in vital signs detection.

3. THROUGH-THE-WALL MIMO IMAGING MODEL OF VITAL SIGNS

3.1. Imaging Model of Wall

Depending on the way that antennas are used, MIMO bioradar systems are classified as air-coupled or wall-coupled systems [22]. The wall-coupled system's antenna is in full contact with the wall, but the antenna array of the air-coupled MIMO system is deployed away from the wall. Also, air-coupled MIMO system is more flexible since the antenna array can be set parallel or unparallel to the wall. Therefore, the air-coupled systems are discussed in this paper.

As Path 1 in Fig. 2 shows, EM waves derived from the mth transmitting channel propagate in the air, and then part of the EM energy is reflected back by the front surface of wall. Some of the reflected EM waves that arrive at the nth receiving antenna form the echo. That is to say, the whole propagation path of EM waves reflected by the front edge is in the air. Some of the EM waves propagate into the wall, refract at the front surface, reflect on the rear surface and finally arrive at the nth receiving antenna (As depicted in Path 2). Path 3 shows another kind of propagation paths which can be called high-order transmission path. But the propagation length of Path 3 is much longer than Path 2, and its attenuation caused by wall medium is much stronger. Actually, reflection and refraction of the EM waves occur at each air-to-wall interface or each wall-to-air interface. Therefore, multi-reflections of EM waves in the wall will disperse the energy and cause amplitude attenuation of EM waves. High-order transmission waves are weak and often neglected due to the amplitude attenuation. Thus, the main echoes of the wall are mainly from the front and rear surfaces, respectively.

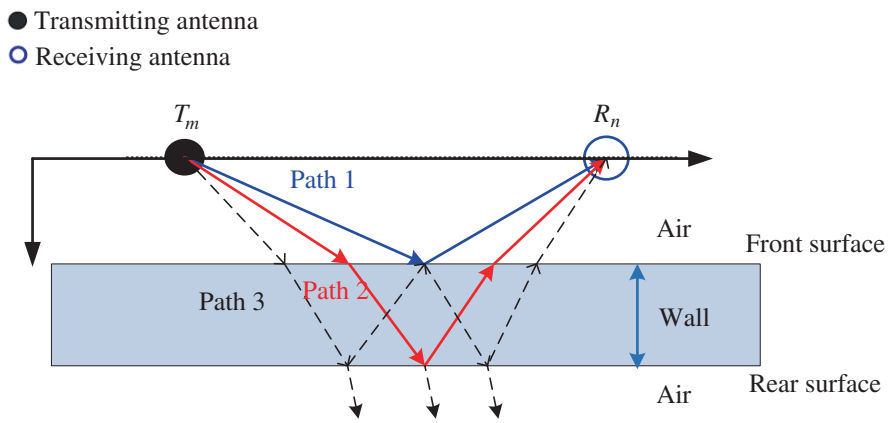

Figure 2. Propagation model of wall for the air-coupled MIMO system.

3.2. TWI Model of Vital Signs

Assuming that the UWB MIMO radar antenna array is arranged along the direction parallel to the wall, the through-the-wall propagation procedure of MIMO channels is shown in Fig. 3(a). Neglecting the high-order transition waves depicted in dashed lines, only parts of the transmitting EM waves sound targets behind the wall and reflected by the human body, which is depicted as the solid line. The propagating path from the human to the nth receiving antenna is similar to the transmitting path. It also includes multiple reflections and multiple refractions. EM waves propagate in the wall medium at a speed of $v = c/\sqrt{\varepsilon}$, where ε is the dielectric constant of the wall. As a result, the electrical length in the wall is not consistent to propagation distance in free space.

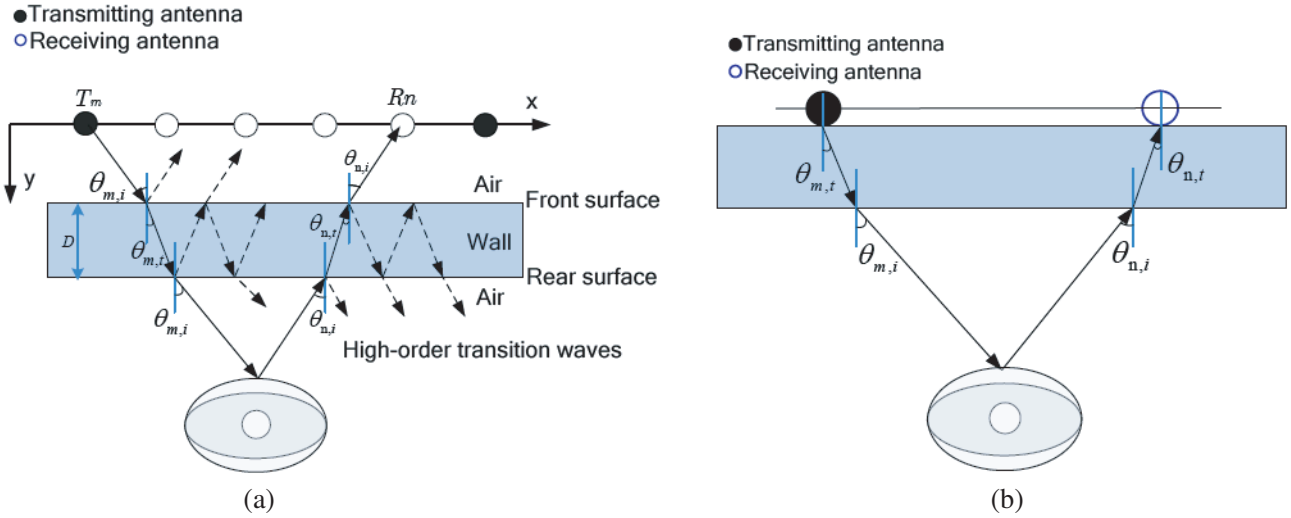

Figure 3. Propagation model through single wall. (a) Propagation model in practical situation. (b) Simplified propagation model.

According to [19] and [23], the three-layer model including air to wall and wall to air can be simplified to be a two-layer model of wall to air described as in Fig. 3(b). But we need to pay attention to that the above simplification is only for the computation convenience of equivalent electrical length. The reflected EM waves of the front wall edge still propagate in the air.

Since MIMO bioradar is performed in bistatic mode, the computation of the total electrical length

is modified as

$$EL_{m,n}(x,y) = l_{m,n}(x,y) + D\left(\sqrt{\varepsilon - \sin^2[\theta_m(x,y)]} - \cos[\theta_m(x,y)]\right) + D\left(\sqrt{\varepsilon - \sin^2[\theta_n(x,y)]} - \cos[\theta_n(x,y)]\right) \quad (5)$$

where D is the thickness of the wall, $\theta_m(x,y)$ the incident angle between the mth transmitting antenna and the pixel (x,y), and $\theta_n(x,y)$ the incident angle between the nth receiving antenna and the pixel (x,y). $\theta_m(x,y)$ and $\theta_n(x,y)$ can be estimated as

$$\begin{aligned} \theta_m(x,y) &= ac\tan\left(\left|\frac{y - y_{T_m}}{x - x_{T_m}}\right|\right) \\ \theta_n(x,y) &= ac\tan\left(\left|\frac{y - y_{R_n}}{x - x_{R_n}}\right|\right) \end{aligned} \quad (6)$$

We can substitute Eq. (5) for Eq. (4) to get a focused imagery of human with accurate wall parameters. In the above analysis, the dielectric lengths of transmitting path and receiving path are computed, respectively. Then, it is not necessary to arrange the antenna array parallel to the wall.

4. AUTOFOCUSING OF VITAL SIGNS TWI

A new TWI method for human targets based on modified autofocusing algorithm is proposed as in Fig. 4. The main procedures are as follows.

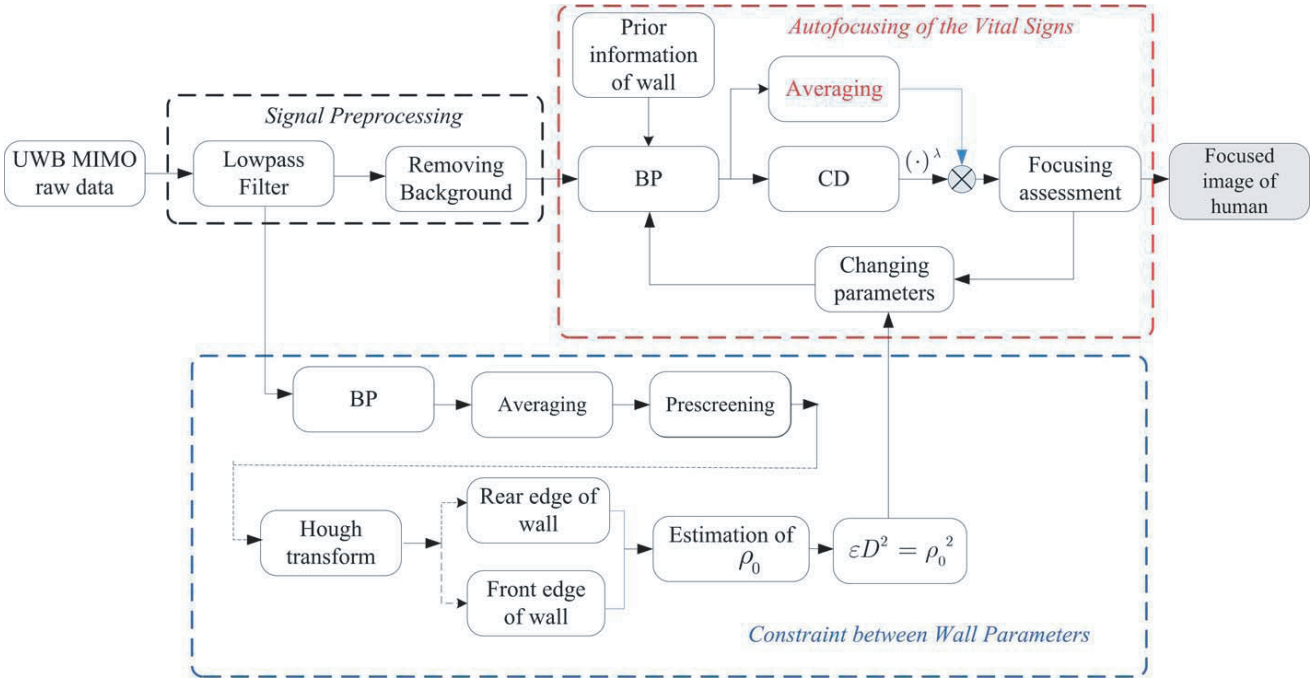

Figure 4. Flow chart of the proposed TWI method.

4.1. Signal Preprocessing

In TWI of human vital signs, the imaging subjects can be divided into two types of objects which are micro-motion vital signs and stationary building structures. Obviously, the preprocessing methods of these two types of objects are different. For vital signs detection, reflection of the wall is considered as

the interference. Therefore, the background removal is often used for suppressing static clutters formed by the wall. However, for imaging building structure, the signal preprocessing should not include the background removing. Then only lowpass filter and the averaging computation are adopted to preserve and enhance the reflections of wall.

4.2. Constraint between Wall Parameters

The wall is simplified to a uniform medium, so the relevant parameters of the wall include the thickness and the dielectric constant as depicted above. Although there are only two parameters, the computation burden is still heavy in autofocusing step considering that these two parameters are estimated independently. Obviously, it is beneficial to find a constraint between these parameters. The main idea is that the relationship between ε and D can be established by estimating the time duration of EM waves propagating in the wall by the following steps.

4.2.1. Step 1: Averaging

To preserve the static reflection of wall edges, low-pass filtering along slow-time domain is adopted instead of background removing operation. In this paper, a simple processing of average operation is used. After the average operation, the BP image sequence is projected to one image $I_M(i,j)$ on range-cross-range plane in which the wall is enhanced. i and j are the index number along the cross-range and range direction.

4.2.2. Step 2: Prescreening

Prescreening is performed to suppress the noise and clutters. The pixel values smaller than the global threshold of T_g will be replaced by zero; otherwise, the pixels keep the original values. T_g is determined as

$$\frac{N\left[I_M(i,j) < T_g\right]}{N\left[I_M(i,j)\right]} = \gamma \tag{7}$$

where $N[\cdot]$ is the operation of computing the number of elements which meets the given condition in braces. γ is selected to be 0.5 according to the experience.

4.2.3. Step 3: Hough Transform

The reflection from the front edge of the wall presents as a line in BP image, because EM waves reflected from the front edge propagate into the air and are not affected by wall medium. Strictly speaking, the reflection from the rear edge of wall is an arc due to the defocusing propagating effect in wall medium. However, it can be seen as a line approximately compared with the other strong reflections in the image.

Hough Transform (HT) is a commonly used algorithm to automatically extract the line structures in image and used in our method. HT maps a line on Cartesian coordinates in the image, which is depicted as $y = kx + b$, to a point on the (ρ, θ) plane by

$$\rho = x\cos\theta + y\sin\theta \tag{8}$$

where ρ is the distance from the origin to the closest point on the straight line, and θ is the angle between the axis and the line connecting the origin with that closest point.

4.2.4. Step 4: Estimation of the Electrical Length in the Wall

For the case of single wall, two edges of wall approximately lead to two lines in BP image, so two extreme points (ρ_1, θ_1) and (ρ_2, θ_2) can be searched in HT space. Ordinarily, these two edges of wall in normal building structures are approximately parallel. So θ angles of the two extreme points are close which can be depicted as $\theta_1 \approx \theta_2$. The distance of the two lines in (x, y) plane can be estimated as $\rho_0 = |\rho_1 - \rho_2|$.

4.2.5. Step 5: Building the Constraint Relationship of Parameters

According to the speed EM waves propagating in the wall medium, the constraint relationship between D and ε is defined as

$$\varepsilon D^2 = \rho_0^2 \tag{9}$$

Therefore, the electrical length depicted in Formula (5) is simplified into a function with one variable (D or ε). The focused image can be obtained by estimating only one parameter in autofocusing step.

4.3. Autofocusing of the Vital Signs

4.3.1. Enhancement of Vital Signs

It is of significant importance to select suitable prominent objects. In our case, getting focused image of vital signs is considered as the main aim of the autofocusing procedure. Thus, the vital signs should be chosen as the prominent objects for autofocusing in this paper. And the focusing performance of vital signs is scored to assess the image focusing performance and the estimation accuracy of parameters in the autofocusing procedure.

SNCR of vital signs is low compared with the static building structure or clutters due to the attenuation effect of wall. In addition, channel number used in coherent superposition for UWB MIMO bioradar is limited compared with SAR imaging, so SNCR of vital signs in MIMO image will be further declined. If neglected, this problem will decline accuracy of focusing performance assessment.

Besides background removing in preprocessing step, change detection (CD) algorithm is implemented to further enhance the vital signs as follows [14, 24].

$$I(i,j) = \left(\sum_{l=0}^{L-1} \left| I(i,j,l) - \sum_{l=0}^{L-1} |I(i,j,l)|/L \right|^2 \right) \cdot \left(\sum_{l=0}^{L-1} |I(i,j,l)| \right)^{\lambda} \tag{10}$$

where l is the samples indexed along slow time, L the total number of the slow time samples in the BP image sequence, and λ the relaxation factor which controls the enhancement of vital signs. For each pixel sequence, the change part will be reserved and accumulated. The stationary part will be seen as mean value and removed by variation operation. Therefore, the vital signs with micro-motion are enhanced.

4.3.2. Focusing Assessment

The vital signs after CD can be seen as point-like targets in BP image [14]. According to [25], the kurtosis is proved to be a suitable metric to describe the contrast of an image mainly with point-like targets, and it is defined as

$$Ku[I_D] = \frac{\sum_{i=1}^{P} \sum_{j=1}^{Q} (|I_D(i,j)| - \mu)^4}{(PQ-1)\sigma^4} - 3 \tag{11}$$

where P and Q are the pixel numbers along range and cross-range dimension; μ and σ are the mean and the standard deviation of the image; I_D is the image formed by parameter value D.

4.3.3. Iterative Procedure

The parameters are changed iteratively to form images with different focusing performances. By building the constraint between wall parameters, the number of parameters is reduced to one. Our aim is to estimate the best wall parameters by making Formula (11) get the maximum value,

$$\tilde{D}_i = \arg\max_{D_i} Ku[I_D] \tag{12}$$

In this paper, we simply go through all the samples of D parameter ranging from 0 m to 0.5 m with a fixed interval. The D value corresponding to the maximum value of kurtosis is considered as the optimal parameter and used for calibration of the wall parameters.

5. SIMULATED RESULTS

5.1. Measurement Setup

The received echo of the vital signs for a UWB MIMO system was calculated by finite-difference time-domain (FDTD) method. As depicted in Fig. 5, the human chest is simulated by a 2D real magnetic resonance imaging (MRI) slice. The organs inside the chest are set to different dielectric constant values according to the database of virtual human [26]. The maximum displacement of chest wall along the line of sight during breathing is about 4 millimeters. 45 MRI slices are sampled during two whole respiration periods, and MIMO bioradar echoes of each MRI slice can be obtained to simulate the echoes of vital signs with micro-motion. The uniform linear MIMO array is composed of two transmitting elements settled at the center of the array and 38 receiving elements with interval space of 0.05 m. The transmitted signal was impulse waveform with a width of 5 ns. The center of the MIMO array is set to be origin of the coordinate system. A uniform wall with certain thickness (0.2 m or 0.3 m), ε of which is 6.25, is arranged 1.1 m away from the antenna array. The wall is 2 m long and parallel to antenna array. White Gaussian noise with a 25 dB signal-to-noise ratio is added to the raw data.

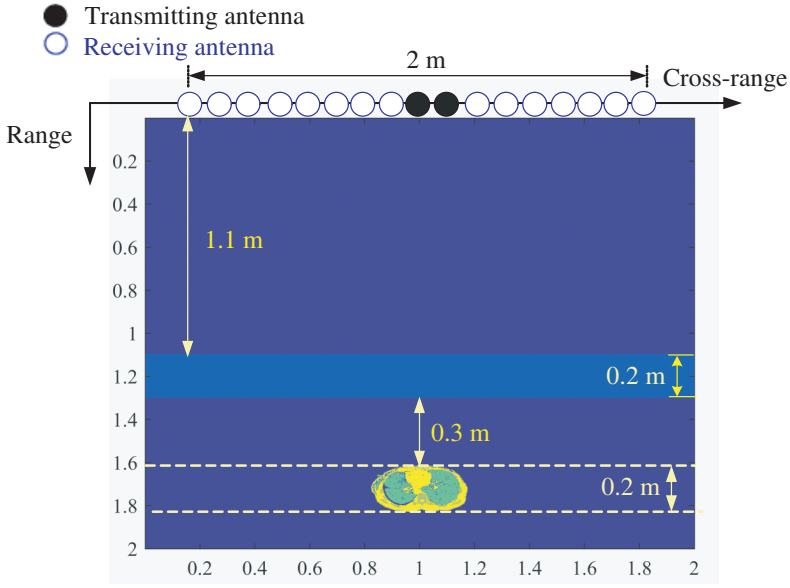

Figure 5. Schematic figure of simulated scene containing single person.

5.2. Imaging of Single Human Vital Sign

The range and cross-range coordinates of the front point of chest wall are 1.6 m and 0 m (as Fig. 5 shows). BP image without calibration or removing background is given in Fig. 6. The image of the front edge of wall is a line structure, since the EM waves reflected by it propagate in free space. However, the rear edge is defocused to an arc structure. If we use HT on this BP image, the rear edge cannot be ideally mapped to one ideal point but multiple points in an area instead (as shown in Fig. 7). Position of the rear edge can be approximately extracted as the point with the biggest amplitude in this area of HT space. The propagation range of EM waves in the wall can be estimated to be about 0.52 m by the positions of two edges. Accordingly, the relationship between parameters is $\varepsilon D^2 = 0.52^2$. As a result, the imaging model is relevant to only D. Kurtosis of the image with D is given in Fig. 8. Kurtosis gets the maximum value when estimation is close to the real value of D. D value corresponding to the maximum Kurtosis is set as the calibration parameter in BP imaging. We ran the program on the MATLAB 2011a by ordinary desktop PC. Autofocusing with two-dimensional search of D and ε needs 1848.5 s. But autofocusing with the proposed processing procedure needs only 189.7284 s. So, we can

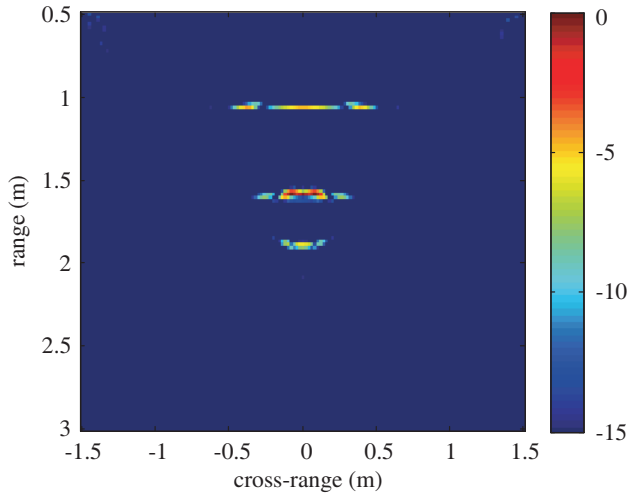

Figure 6. Image without calibration or removing background.

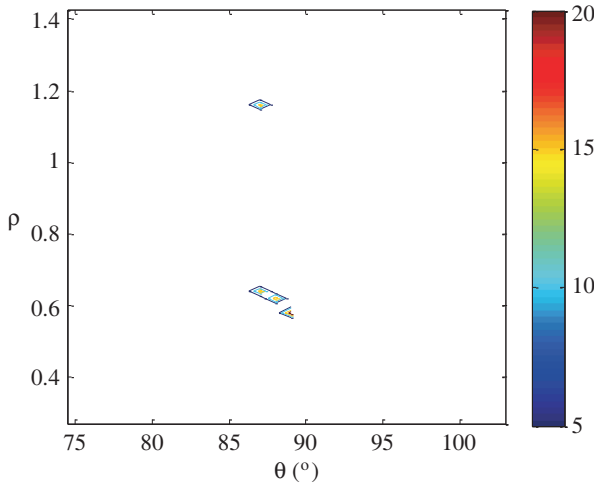

Figure 7. Hough transform result.

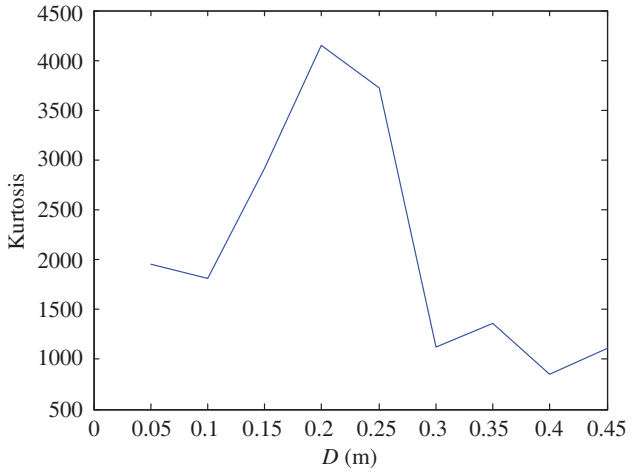

Figure 8. Kurtosis of the image with different D.

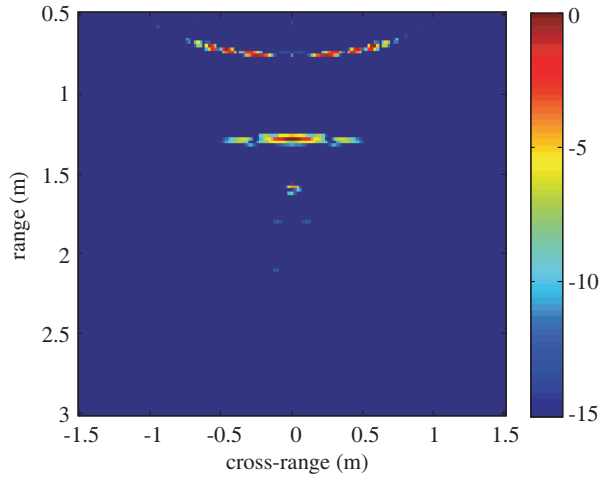

Figure 9. Image with calibration and removing background.

observe the proposed method's improvement of efficiency. Parallel optimization or advanced processing platform can be used to further improve the real-time performance of the proposed method.

After autofocusing step, the rear edge is focused as a line, and the vital sign is focused to be a point, but the front edge is defocused to be an arc (as Fig. 9). For the case of single wall, the front edge should not be calibrated. The imaging procedures of the two edges should be different. Without calibration of wall parameters, vital signs are defocused due to the influence of wall medium (as shown in Fig. 10). After the calibration of wall parameter, the vital sign is focused to a point approximately (as Fig. 11 shows).

It is worth noticing that the reflections of wall can be suppressed by the processing steps such as removing background and CD. Without wall parameters calibration the amplitude of wall edges are about 0 dB and -3.557 dB, but the amplitude of vital sign is much smaller than the former one at about -16.16 dB (as shown in Table 1). Although wall parameters are not calibrated, the static wall reflections are suppressed, and the vital signs are enhanced to be 0 dB by removing background and CD. If the vital sign is well focused, the amplitude of vital signs is larger than the wall edges without background removing processing or CD. Certainly, combining background removing, CD with

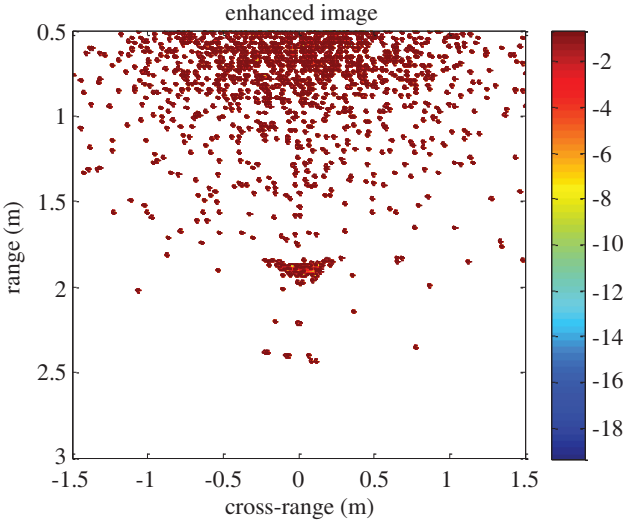

Figure 10. Image of vital signs of human after CD without calibration of wall parameters.

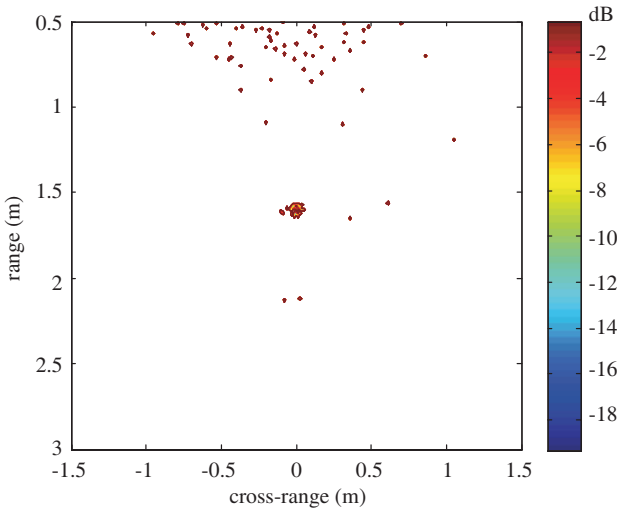

Figure 11. Image of vital signs after CD with calibration of wall.

Table 1. Comparison of results with different processing steps.

Used processing procedure		Front edge (dB)	Rear edge (dB)	Vital sign (dB)
Without wall parameters calibration	Without background removing or CD	0	−3.56	−16.16
	With background removing and CD	−17.7 (average of noise points)	−17.7 (average of noise points)	0
With wall parameters calibration	Without background removing or CD	−3.63	−2.70	0
	With background removing and CD	−19.8 (average of noise points)	−19.8 (average of noise points)	0

wall parameters calibration together, the vital sign achieves the highest focusing quality.

The improvement of focusing quality can improve the SNCR of vital signs. The SNCR is defined as

$$\mathrm{SNCR} = 10\lg\frac{P_t}{P_c} = 10\lg\frac{\sum\limits_{(i,j)\in\chi_t}|I(i,j)|^2/N_t}{\sum\limits_{(i,j)\in\chi_c}|I(i,j)|^2/N_c} \tag{13}$$

where P_t is the pixel power in the vital signs region χ_t; P_c is the pixel power in the clutter and noise region χ_c; N_t and N_c are the pixel numbers in χ_t and χ_c.

The SNCR of the vital sign before compensation of wall parameters in Fig. 10 is 9.6498 dB, and the SNCR of the vital sign after compensation reaches 22.9948 dB. From this result, we can conclude that the clutters and noise can be mitigated. The improvement of the SNCR is beneficial for enhancing the detection performance.

5.3. Imaging of Multiple Human Vital Signs

In this simulation, the range and cross-range coordinates of 3 human vital signs are (1.7 m, 0 m), (2.407 m, 0.5 m) and (2.407 m, −0.5 m) (as Fig. 12 shows). When there are multiple humans behind the

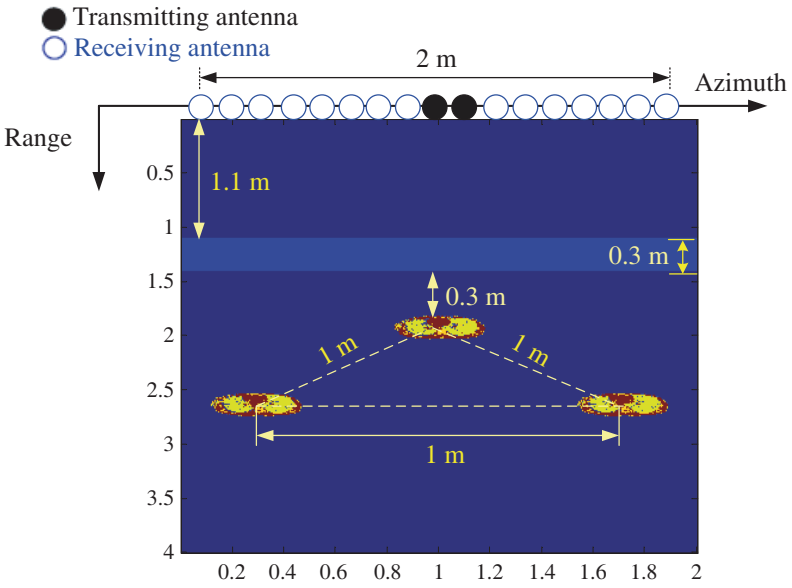

Figure 12. Schematic figure of simulated scene containing three humans.

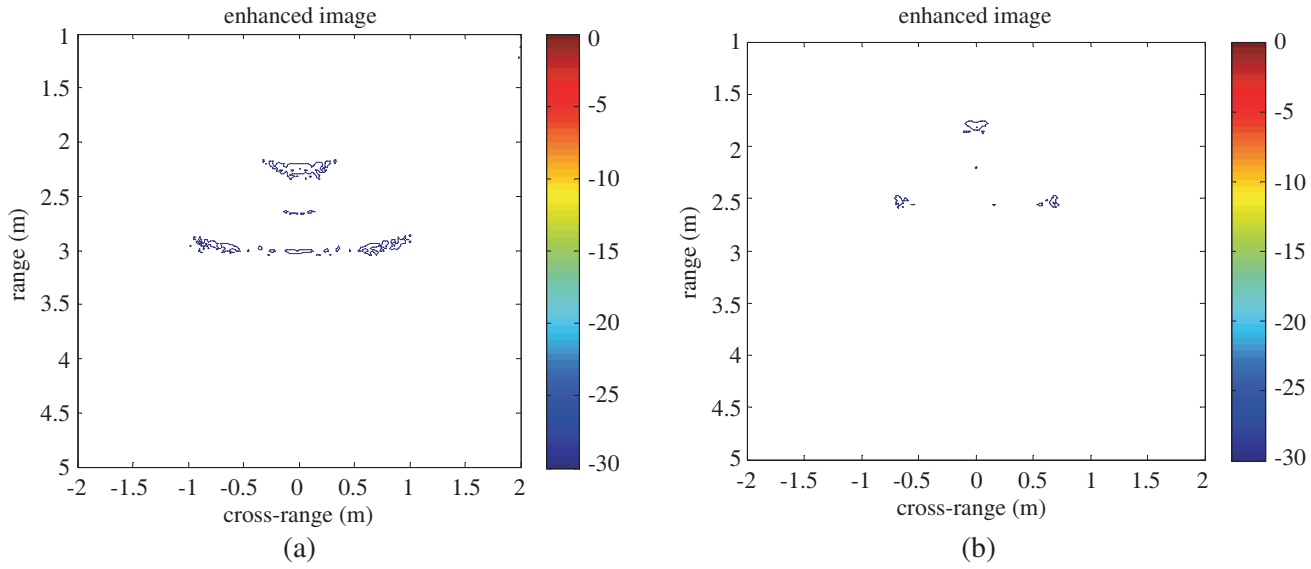

Figure 13. Image of three vital signs. (a) Before wall parameters calibration. (b) After wall parameters calibration.

wall, mutual interferences are inevitable. As shown in Fig. 13(a), images of three vital signs without calibration of wall are blurred, which causes the resolution of image decline and clutters between vital signs strong enough to interrupt the detection. It will be difficult to correctly decide the number of vital signs through the above results. And the positions of vital signs in the BP image deviate from the true positions. After autofocusing, focusing performance improves with the correction of the positions of vital signs (as Fig. 13(b) shows). The clutters caused by mutual interference and low resolution of defocused image are effectively suppressed. From this result, the possibility of detecting three human vital signs increases. So autofocusing method is beneficial for multiple human vital signs detection.

5.4. Imaging of Empty Background without Human Vital Signs

Only a 0.2 m-thick wall is simulated in the scene, and Gauss white noises are added to the raw data. We process the data using the proposed autofocusing method. The kurtosis values of image under different signal-to-noise ratio (SNR) in absence of human being are given in Fig. 14.

Under the non-noise condition, the Kurtosis values are large but obviously fluctuated (as shown in Fig. 14(a)). However, in real world this condition is not reasonable since there are always noises in the environment. Therefore, we simulate the situations with SNR of 5 dB, 15 dB and 25 dB (as shown in Figs. 14(b), (c) and (d)). The trends of Kurtosis values under these situations are not regular. But the common feature of these situations is that the kurtosis values are very small compared with the situations of existing human vital signs which are shown in Fig. 8. Kurtosis values are small because there are not point-like prominent targets in empty scene without human being. This feature can be used to efficiently decide the human vital signs are existed or not.

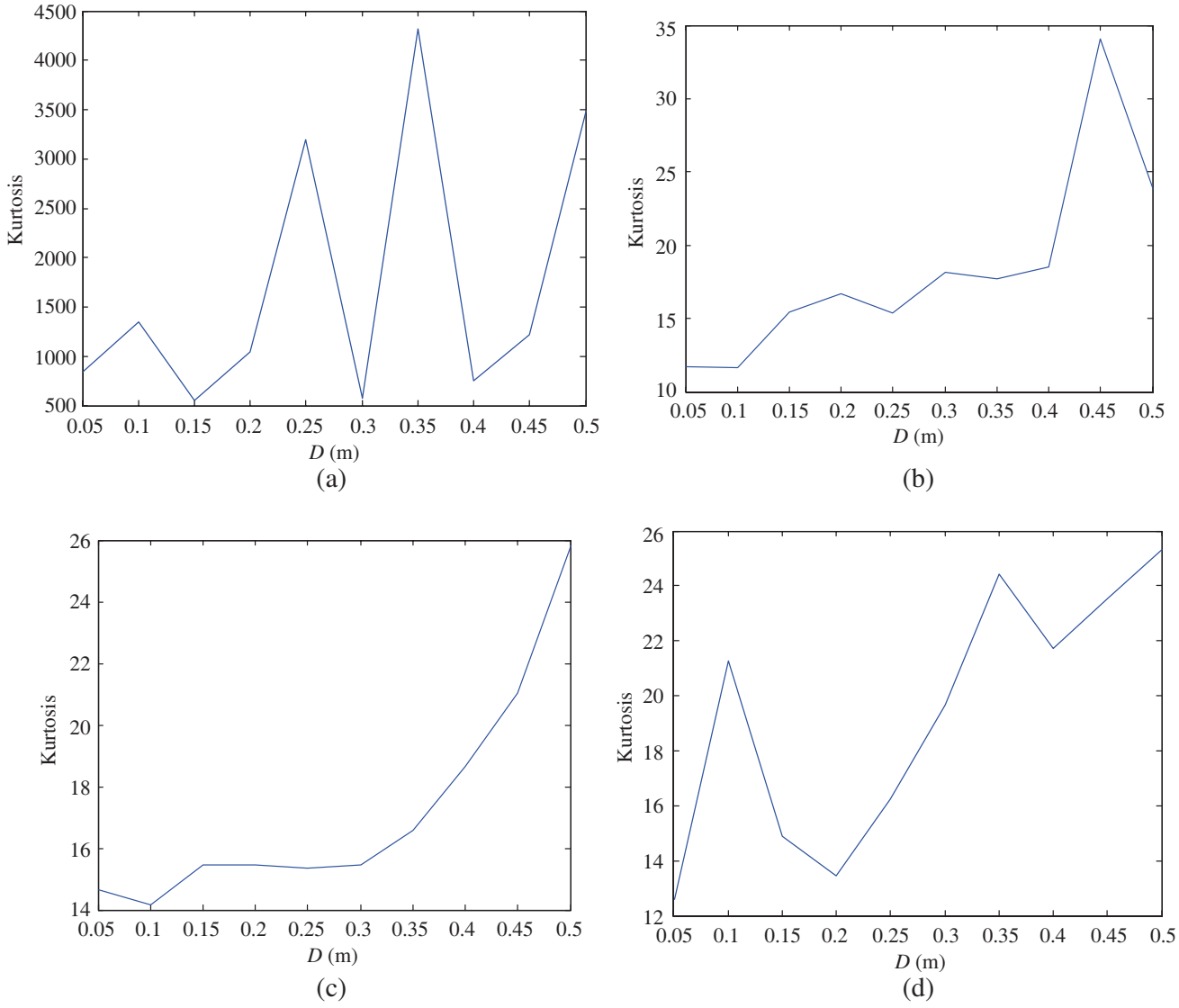

Figure 14. Kurtosis of the image in absence of human being. (a) Non-noise condition. (b) SNR = 5 dB. (c) SNR = 15 dB. (d) SNR = 25 dB.

6. CONCLUSIONS

In applications of vital signs TWI, some phenomena, such as the change of propagating speed and refraction, influence the propagating path of EM waves and focusing performance of the image. If uncompensated, the vital signs will be defocused, and the SNCR of human vital signs will deteriorate. When there are multiple humans in the image area, the blurred image will make detection of humans much harder. The above phenomena challenge the vital signs detection and location. A novel autofocusing procedure of human vital signs is proposed in this paper. To improve the efficiency of the autofocusing method, a constraint relationship of wall parameters is built according to the priori information of wall. The simulated results validate the proposed method. When several walls exist in the environment, calibration parameters of vital signs behind different walls are obviously different. The segmentation of image area and calibration parameters estimation of each area is necessary and considered as our future job.

ACKNOWLEDGMENT

This work was supported by the National Natural Science Foundation of China (No. 61327805) and Natural Science Foundation of Shaanxi Province (No. 2017JQ6009).

REFERENCES

1. Li, J., L. B. Liu, Z. F. Zeng, and F. S. Liu, "Advanced signal processing for vital sign extraction with applications in UWB radar detection of trapped victims in complex environments," *IEEE J. Sel. Top. Appl. Earth Obs. Remote Sens.*, Vol. 7, 783–791, 2013.
2. Chen, K. M., D. Misra, H. E. Wang, H. R. Chuang, and E. Postow, "An X-band microwave life-detection system for searching human subjects under earthquake rubble or behind barrier," *IEEE Trans. Biomed. Eng.*, Vol. 47, 105–114, 2000.
3. Li, Z., W. Z. Li, H. Lv, Y. Zhang, X. J. Jing, and J. Q. Wang, "A novel method for respiration-like clutter cancellation in life detection by dual-frequency IR-UWB radar," *IEEE Trans. Microw. Theory Tech.*, Vol. 61, 2086–2092, 2013.
4. Lan, F. Y., L. J. Kong, X. B. Yang, and Y. Jia, "Life-sign detection of through-wall-radar based on fourth-order cumulant," *Proceedings of the Radar Conference (RADAR)*, Xi'an, China, Apr. 14–16, 2013.
5. Ren, L. Y., Y. S. Koo, H. F. Wang, Y. Z. Wang, Q. H. Liu, and A. E. Fathy, "Noncontact multiple heartbeats detection and subject localization using UWB impulse Doppler radar," *IEEE Microwave and Wireless Components Letters*, Vol. 25, No. 10, 690–692, 2015.
6. Wang, F., T. Horng, K. Peng, J. Jau, J. Li, and C. Chen, "Detection ofconcealed individuals based on their vital signs by using a see-through-wall imaging system with a self-injection-locked radar," *IEEE Trans. Microw. Theory Techn.*, Vol. 61, No. 1, 696–704, 2013.
7. Liu, L. B. and S. X. Liu, "Remote detection of human vital sign with stepped-frequency continuous wave radar," *IEEE J. Sel. Top. Appl. Earth Obs. Remote Sens.*, Vol. 7, 775–782, 2014.
8. Ram, S. S. and A. Majumdar, "High-resolution radar imaging of moving humans using doppler processing and compressed sensing," *IEEE Transactions on Aerospace and Electronic Systems*, Vol. 51, No. 2, 1279–1287, 2015.
9. Hu, J., Y. P. Song, T. Jin, B. Y. Lu, G. F. Zhu, and Z. M. Zhou, "Shadow effect mitigation in indication of moving human behind wall via MIMOTWRI," *IEEE Geoscience and Remote Sensing Letters*, Vol. 12, No. 3, 453–457, 2014.
10. Melamed, R. and N. Chayat, "Apparatus and method for doppler-assisted MIMO radar microwave imaging," United States Patent Application, 20110237939, US, 2013.
11. Ram, S. S. and A. Majumdar, "Through-wall propagation effects on Doppler-enhanced frontal radar images of humans," *IEEE Radar Conference*, 1–6, 2016.

12. Wang, F. K., T. S. Horng, K. C. Peng, J. K. Jau, J. Y. Li, and C. C. Chen, "Detection of concealed individuals based on their vital signs by using a see-through-wall imaging system with a self-injection-locked radar," *IEEE Trans. Microw. Theory Techn.*, Vol. 61, No. 1, 696–704, 2013.
13. Hunt, A. R., "Use of a frequency-hopping radar for imaging and motion detection through walls," *IEEE Transactions on Geoscience and Remote Sensing*, Vol. 47, No. 5, 1402–1408, 2009.
14. Liang, F. L., F. G. Qi, Q. An, H. Lv, F. M. Chen, Z. Li, and J. Q. Wang, "Detection of multiple stationary humans using UWB MIMO radar," *Sensors*, Vol. 16, No. 11, 2016.
15. Qu, Y., G. Liao, S.-Q. Zhu, X.-Y. Liu, and H. Jiang, "Performance analysis of beamforming for MIMO radar," *Progress In Electromagnetics Research*, Vol. 84, 123–134, 2008.
16. Zhuge, X. D. and A. G. Yarovoy, "Study on two-dimensional sparse MIMO UWB arrays for high resolution near-field imaging," *IEEE Transactions on Antennas and Propagation*, Vol. 60, No. 9, 4173–4182, 2012.
17. Muqaibel, A. H. and A. Safaai-Jazi, "A new formulation for characterization of materials based on measured insertion transfer function," *IEEE Trans. Microw. Theory Tech.*, Vol. 51, No. 8, 1946–1951, 2003.
18. Muqaibel, A. H., A. Safaai-Jazi, A. Bayram, A. M. Attiya, and S. M. Riad, "Ultrawideband through-the-wall propagation," *IEE Proc. Microw. Antennas Propag.*, Vol. 152, No. 6, 581–588, 2005.
19. Jin, T., B. Chen, and Z. M. Zhou, "Image-domain estimation of wall parameters for autofocusing of through-the-wall SAR imagery," *IEEE Transactions on Geoscience and Remote Sensing*, Vol. 51, No. 3, 1836–1843, 2013.
20. Wang, G. Y. and M. G. Amin, "Imaging through unknown walls using different standoff distances," *IEEE Transactions on Signal Processing*, Vol. 54, No. 10, 4015–4025, 2006.
21. Ahmad F., M. G. Amin, and G. Mandapati, "Autofocusing of through-the-wall radar imagery under unknown wall characteristics," *IEEE Trans. Image Process.*, Vol. 16, No. 7, 1785–1795, 2007.
22. Al-Qadi, I. L. and S. Lahouar, "Measuring layer thicknesses with GPR theory to practice," *Construction and Building Materials*, Vol. 19, No. 10, 763–772, 2005.
23. Aftanas, M., J. Rovnakova, M. Drutarovsky, and D. Kocur, "Efficient method of TOA estimation for through wall imaging by UWB radar," *Proc. Int. Conf. Ultrawideband*, 101–104, 2008.
24. Amin, M. G. and F. Ahmad, "Change detection analysis of humans moving behind walls," *IEEE Transactions on Aerospace and Electronic Systems*, Vol. 49, No. 3, 1410–1425, 2013.
25. Liang, F. L., M. Liu, H. N. Li, F. G. Qi, Z. Li, and J. Q. Wang, "Through-the-wall imagery of human vital signs using UWB MIMO bioradar," *2017 IEEE 2nd Information Technology, Networking, Electronic and Automation Control Conference (ITNEC)*, 924–927, Chengdu, China, Dec. 15–17, 2017.
26. Gabriel, C.. "Compilation of the dielectric properties of body tissues at RF and microwave frequencies," Technical Report, 78235-5102, Brooks Air Force Base, Texas, 1996.